AIAA JOURNAL
Vol. 48, No. 1, January 2010

Thermal Force and Moment Determination of an Integrated Thermal Protection System

Oscar A. Martinez,* Anurag Sharma,† Bhavani V. Sankar,‡ and Raphael T. Haftka§
University of Florida, Gainesville, Florida 32611
and
Max L. Blosser¶
NASA Langley Research Center, Hampton, Virginia 23681

DOI: 10.2514/1.40678

This paper is concerned with homogenization of a corrugated-core sandwich panel, which is a candidate structure for integral thermal protection systems for space vehicles. The focus was on determination of thermal stresses in the face sheets and the web caused by through-the-thickness temperature variation. A micromechanical method was developed to homogenize the sandwich panel as an equivalent orthotropic plate and calculate the equivalent thermal forces and moments for a given temperature distribution. The same method was again used to calculate the stresses in the face sheets and the core. The method was demonstrated by calculating stresses in a sandwich panel subjected to a temperature distribution described by a quartic polynomial in the thickness direction. Both constrained and unconstrained boundary conditions were considered. In the constrained case the plate boundaries are constrained such that there are no deformations in the macroscale sense. The unconstrained case assumes that there are no force and moment resultants in the macroscale. The results for stresses are compared with that from a three-dimensional finite element analysis of the representative volume element of the sandwich structure, and the comparison was found to be within 5% difference. The micromechanical analysis, which is less time consuming, will be useful in the design and optimization of integral thermal protection system structures.

Nomenclature

$\{D\}^{(e)}$	=	deformation vector of the eth component (micro deformation)
$\{D\}^{M}$	=	deformation vector of the unit cell (macrodeformation)
d	=	height of the sandwich panel (centerline to centerline)
e	=	component index of the corrugated core
$F_i^{(m)}$	=	nodal force on the finite element method model
l	=	length of the cantilever beam
Q_{ij}	=	transformed lamina stiffness matrix
Q_x, Q_y	=	shear force on the unit cell
s	=	web length
$[T_D]^{(e)}$	=	deformation transformation matrix of the ith component of the corrugated core
t_{BF}	=	bottom face sheet thickness
t_{TF}	=	top face sheet thickness
t_w	=	web thickness
U	=	unit cell strain energy
$\bar{y}$	=	local axis of the web
ΔT	=	temperature distribution in the integral thermal protection system
ε_o	=	midplane strain
θ	=	angle of web inclination
κ	=	curvature
$\tau_{\bar{x}\bar{y}}$	=	local shear stress in the webs
$2p$	=	unit cell length

Received 28 November 2008; revision received 7 August 2009; accepted for publication 5 September 2009.

*Structural Analyst, Jacobs Engineering, Engineering Science Contract Group.
†Graduate Student, Department of Mechanical and Aerospace Engineering. Student Member AIAA
‡Newton C. Ebaugh Professor, Department of Mechanical and Aerospace Engineering. Associate Fellow AIAA.
§Distinguished Professor, Department of Mechanical and Aerospace Engineering. Fellow AIAA.
¶Aerospace Technologist, Metals and Thermal Structures Branch.

I. Introduction

REDUCING the cost of launching a spacecraft is one of the critical needs of the space industry. Government and private corporations use space for various objectives such as reconnaissance, communications, weather monitoring, military, and other experimental purposes. With every launch the government or corporation spends a significant amount of money to launch their payload into space. One of NASA's goals is to reduce the cost of delivering a pound of payload into a low Earth orbit by an order of magnitude [1]. One of the most expensive systems of a space vehicle is the thermal protection system (TPS) [2], which protects the space vehicle from the extreme planetary reentry temperatures. Hence, reducing the cost of the TPS could offer significant reduction in overall launch cost. The TPS's performance is critical for successful operation of a spacecraft during planetary reentry.

In the next 20 year NASA plans to send manned space missions to Mars. The aerocapture approach will be used to slow down the space vehicle's velocity as it approaches the planetary atmosphere. Aerocaputre technology uses the planet's atmosphere to alter the space vehicle's velocity. The vehicle makes a single pass deep into the planetary atmosphere, using drag to establish a capture orbit. Aerocapture does not use any propellent for the deceleration of the space vehicle, therefore a fuel-free entry method could reduce the typical mass of a space vehicle by half. This reduction in mass allows for cheaper and smaller space vehicles for interplanetary voyages. The aerocapture technology will have an impact on the space vehicle's TPS because of the excessive aerdoynamic heating from the atmospheric friction.

In addition to protection from the exteme reentry temperature, the TPS must satisfy certain general requirements. During ascent and reentry, the TPS has to withstand temperatures ranging from 650 to 1700 K depending on its position on the vehicle. Because the TPS forms the outermost surface of the vehicle, it needs to maintain the aerodynamic shape of the vehicle without excessive deformation, provide adequate insulation to keep the underlying structure within

acceptable temperature limits, and be lightweight. The TPS is also required to be extremely robust, damage-tolerant, and maintain its configuration to effectively perform its primary task of thermal protection.

The Space Shuttle's current TPS technology consists of different types of materials, such as ceramic tiles and blankets, that are distributed all over the spacecraft. This technology makes the space vehicle's exterior very brittle, susceptible to damage from small impact loads, and high in maintenance time and cost. To overcome these difficulties, scientists at NASA developed a metallic advanced-adapted, robust, metallic, operable, reusable (ARMOR) TPS [3,4]. However, the ARMOR TPS's load-bearing capabilities are limited, because large in-plane loads cannot be accommodated under this design, and it has a complicated geometry.

New TPS concepts are currently being investigated by using recently developed metallic foams and also innovative core materials, such as corrugated and truss cores. The integral TPS/structure (ITPS) design can significantly reduce the overall weight of the vehicle as the TPS/structure performs the load-bearing function as well as the thermal protection (see Fig. 1). Sandwich structures provide high stiffness with relatively lighter weight when compared with widely used monolithic and laminated structures. The top face sheet of the TPS panel must withstand temperatures up to 1700 K, C/SiC textile composites are suitable for such applications. The bottom face sheet is not subjected to extremely high temperatures and therefore it can be made from graphite/epoxy textile composites.

Composite corrugated core sandwich structures will be investigated in this paper for use in multifunctional structures for future space vehicles (Fig. 1). This type of ITPS would insulate the vehicle from aerodynamic heating as well as carry primary vehicle loads. The advantages of using such a structure are that it is lightweight and multifunctional. For example, an ITPS configuration offers insulation as well as load-bearing capabilities, require low maintenance, and the panels can be large in size, thus reducing the number of panels needed. The corrugated core sandwich panel is composed of several unit cells. The unit cell consists of two thin face sheets and an inclined web made up of composite laminates. The composite corrugated core will be filled with Saffil®, which is a nonload-bearing insulation made of alumina fibers. The ITPS will be integrated with the vehicle's structure, which promotes low installation and maintenance costs.

Various researchers such as Lok and Cheng [5], Valdevit et al. [6], and Nordstrand [7] investigated and analyzed metallic truss-core sandwich panels subjected to mechanical loadings. Biancolini [8] derived the equivalent stiffness properties of corrugated boards by performing static condensation of the stiffness matrix obtained using the finite element model of the full panel. Buannic et al. [9] used asymptotic expansion-based analytical method for deriving the equivalent properties of corrugated panel. Because the ITPS will act as a thermal barrier for a space vehicle, a thermal analysis is needed to understand the ITPS's thermal behavior. There has not been any research on the thermoelastic behavior and response of corrugated or truss-core sandwich panels proposed for the ITPS construction.

The objective of the current research was to establish an analytical procedure that determines the thermoelastic behavior of the ITPS when subjected to realistic reentry temperature distributions. The analytical models were compared with an expensive and detailed finite element analysis. The equivalent stiffness parameters of the ITPS are presented and discussed. The ITPS was subjected to a realistic reentry temperature and the corresponding thermal force resultants and moments along with the thermal stresses were derived. A detailed description of the thermal response of the ITPS was shown.

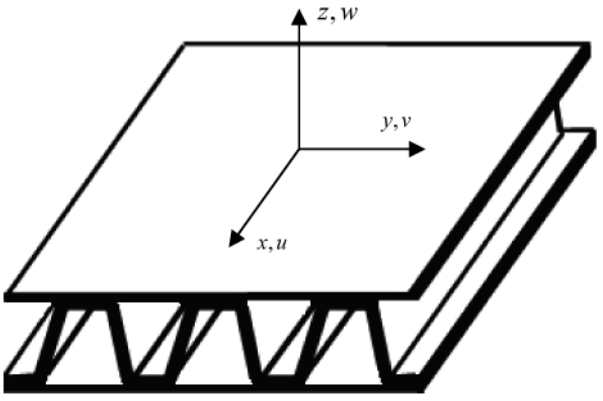

Fig. 1 Corrugated-core sandwich panel.

II. Geometric Parameters

Consider a simplified geometry of an ITPS unit cell shown in Fig. 2. The z axis is in the thickness direction of the ITPS panel. The stiffer longitudinal direction is parallel to the x axis, and y axis is in the transverse direction. The unit cell consists of two inclined webs and two thin face sheets. The unit cell is symmetric with respect to the yz plane. The upper face plate thickness t_{TF} can be different from the lower plate thickness t_{TB}, as well as the web thickness t_w. The unit cell can be identified by six geometric parameters $(p, d, t_{\mathrm{TF}}, t_{\mathrm{BF}}, t_w, \theta)$ (Fig. 2). Four other dimensions (b_c, d_c, s, f) are obtained from geometric considerations. The equations for these relationships are as follows:

$$d_c = d - \frac{1}{2}t_{\mathrm{TF}} - \frac{1}{2}t_{\mathrm{BF}} \tag{1a}$$

$$f = \frac{1}{2}\left(p - \frac{d_c}{\tan\theta}\right) \tag{1b}$$

$$b_c = p - 2f \tag{1c}$$

$$s = \sqrt{d_c^2 + b_c^2} = \frac{d_c}{\sin\theta} = \frac{b_c}{\cos\theta} \tag{1d}$$

The ratio $f/p = 0$ corresponds to a triangular corrugated core, and $f/p = 0.5$ corresponds to a rectangular corrugated core.

III. Analysis

The finite element method is commonly used to determine the response of a sandwich structure. However, the number of nodes and elements needed to properly model the structure can get excessive; as a result a full 3-D finite element analysis is not economical to conduct a preliminary analysis. Such panels may also be represented as a thick plate that is continuous, orthotropic, and homogenous, for which analytical and 2-D finite element method (FEM) solutions [10] are available.

The computational time and effort in determining stiffness and thermal behavior of the ITPS is significantly reduced in comparison with FEM. Analytical models have been proven to be fast, accurate, and suitable for use in preliminary design. It is advantageous to use an analytical model for an optimization procedure. An optimization procedure usually runs about 100 function evaluations per variable, which if done analytically can take minutes rather than hours if done completely with FEM. For example, Bapanapalli et al. [11] used 3-D finite element (FE) analysis of the ITPS in developing response

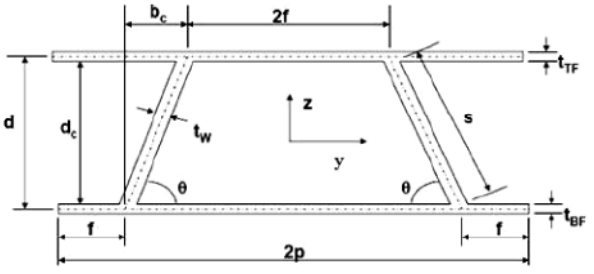

Fig. 2 Dimensions of the unit cell.

surfaces for optimization. Each of the FE analyses took approximately 40 min of wall clock time, whereas the analytical models are expected to take not more than 2 min per analysis. The analytical models are able to provide the designer with an accurate description of the behavior of the ITPS when subjected to realistic reentry temperatures. The thermal moments and force resultants could cause the panel to thermally deflect, buckle, and yield. A TPS must be constrained from deflection to prevent local aerodynamic heating due to the change in the aerodynamic profile. Local buckling is an important design driver of an ITPS because of the thin webs and faces.

The ITPS may be represented as an equivalent thick plate that is continuous, homogenous, and orthotropic with respect to the x and y directions. In the derivation of the stiffness parameters the following assumptions were made:

1) The deformation of the panel is less than 5% when compared with the panel thickness.

2) The panel dimensions in the y direction are 3–6 times larger than the unit-cell width $2p$.

3) The face sheets are thin with respect to the core thickness.

4) The core contributes to bending stiffness in and about the x axis but not about the y axis.

5) The face and web plate laminates are symmetric with respect to their own midplane.

6) The core is sufficiently stiff so that the elastic modulus in the z direction is assumed to be infinite for the equivalent plate. Local buckling of the facing plates does not occur and the overall thickness of the panel is constant.

Previous researchers adopted these assumptions in the derivation of stiffness parameters of sandwich panels with corrugated core (Libove and Hubka [12], C core, Fung et. al. [13], and Z core [14]. The in-plane and out-of-plane stiffness governing the elastic response of a shear-deformable sandwich panel are defined in the context of laminated plate theory incorporating first-order shear-deformable plate theory described by Vinson [15] and Whitney [16]. The appropriate stiffness of the orthotropic plate may be obtained by comparing the behavior of a unit cell of the corrugated-core sandwich panel with that of an element of the idealized homogeneous orthotropic plate (Fig. 3).

The in-plane extensional and shear response and out-of-plane (transverse) shear response of an orthotropic panel are governed by the following constitutive relation:

$$\begin{bmatrix} N \\ Q \\ M \end{bmatrix} = \begin{bmatrix} [A] & & \\ & [C] & \\ & & [D] \end{bmatrix} \begin{Bmatrix} \varepsilon_o \\ \gamma \\ \kappa \end{Bmatrix} \quad \text{or} \quad \{F\} = [K]\{D\} \tag{2}$$

In Eq. (2), ε and γ are the normal and shear strains, κ is the bending and twisting curvatures, $[A]$, $[C]$, and $[D]$ are the extensional, shear, and bending stiffness. The orthotropic plate is assumed to be symmetric.

A. Extensional, Bending, Coupling, and Transverse Shearing Stiffness

Consider a composite corrugated-core unit cell. The unit cell is composed of four components (two faces and two webs), each with its own material properties and ABD matrix; the ABD matrix is composed of three matrices: A is the extensional stiffness matrix, B is the coupling stiffness matrix, and D is the bending stiffness matrix. The ABD matrix of each unit-cell component is combined together in an appropriate manner to create an overall stiffness of the ITPS sandwich panel. The analytical procedure of determining the overall stiffness of the ITPS sandwich panel has been discussed and determined by Martinez et al. [17]. Here we provide a brief description of the analytical method. The overall stiffness of the unit cell was determined by imposing unit midplane strains and curvature (macrodeformation) to the unit cell and then calculating the corresponding midplane strains and curvatures (microdeformations) in each component. The unit-cell components are the two face sheets and two webs. Transformation matrices that relate the macro and microdeformations were derived in the form

$$\{D\}^{(e)} = [T_D]^{(e)}\{D\}^M \tag{3}$$

In Eq. (3), $T_D^{(e)}$ is the deformation transformation matrix that relates macrodeformations to microdeformation, $\{D\}^{(e)}$ is the microdeformation in each component, and $\{D\}^M$ is the macrodeformation in the unit cell (refer to for the transformation matrix), and $e = 1$–4, ($1 =$ top face sheet, $2 =$ bottom face sheet, $3 =$ left web, $4 =$ right web). Using the transformation matrices, the strain energy of each component was determined and added to determine the overall unit-cell strain energy

$$U^{(e)} = \frac{1}{2}(2p)\int_0^s (T_D^e\{D\}^M)^T[\bar{K}]^e(T_D^e\{D\}^M)\mathrm{d}\bar{y} \tag{4}$$

$$U^M = \frac{1}{2}(2p)^2(\{D\}^M)^T[K]\{D\}^M = \sum_{e=1}^{4} U^{(e)} \tag{5}$$

From the strain energy we determined the ITPS sandwich panel stiffness as the sum of the transformed stiffnesses of the components

$$K = \sum_{e=1}^{4} K^{(e)} \tag{6}$$

where

$$K^{(e)} = \frac{1}{2p}\int_0^s T^{(e)T}\bar{K}^{(e)}T^{(e)}\mathrm{d}\bar{y} \tag{7}$$

The details of the derivation and verification of the method using full-scale finite element models are described in Martinez et al. [17].

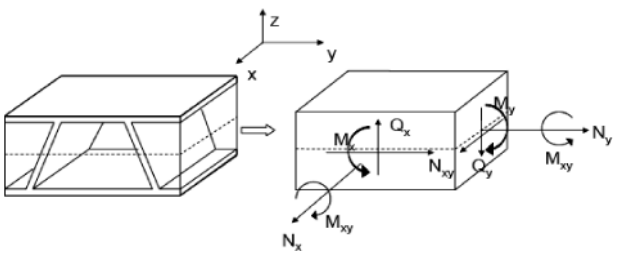

Fig. 3 Equivalent orthotropic thick plate for the unit-cell corrugated-core sandwich panel.

B. Heat Transfer and Temperature Distribution

Thermal analysis of an ITPS involves complex heat transfer mechanisms in severe transient thermal environments. Pressure, conduction, radiation, convection, and temperature variation all play important roles in the thermal performance of an ITPS (Blosser [1]). The proposed ITPS is a multifunctional structure that possesses load-bearing capabilities as well as provides insulation for the space vehicle. During reentry the outer surface of the space vehicle is exposed to extreme reentry temperatures due to the incoming heat flux (see Fig. 4). The heat flux causes the ITPS temperature to rise dramatically, and as a result it causes severe thermal stresses that lead to excessive thermal deflection and even thermal buckling. Knowing the response of the ITPS to a change in temperature is a critical need because panel deflection, buckling (local or global), temperature, and yielding are all critical functions of an ITPS that influence the design.

Consider an orthotropic unit cell of the ITPS with the following dimensions: $p = 50$ mm, $d = 100$ mm, $t_{\mathrm{TF}} = 1$ mm, $t_{\mathrm{BF}} = 1$ mm, $t_w = 1$ mm, $\theta = 75°$, subjected to an incident heat flux versus reentry time of a Space Shuttle-like vehicle (Fig. 4). The corrugated-core sandwich panel is assumed to be made out of graphite/epoxy AS/3501, $E_1 = 138$ GPa, $E_2 = 9$ GPa, $G_{12} = 6.9$ GPa, $\nu_{12} = 0.3$, with four laminas in each component and a stacking sequence of $[90/0]_s$. Typically, simplified one-dimensional models (Dorsey et al. [3]) are used to predict the thermal performance of a thermal protection system when subjected to realistic temperature

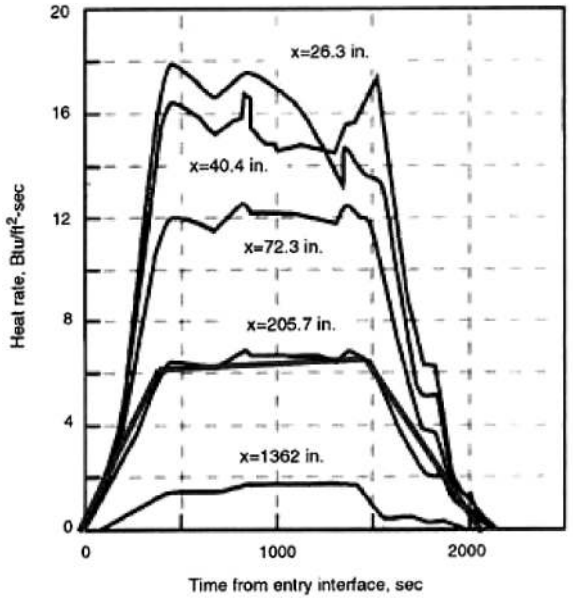

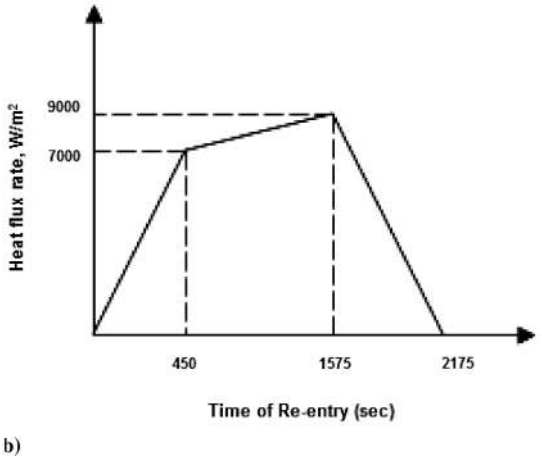

Fig. 4 Heating profiles for a Shuttle-like vehicle obtained from Dorsey et al. [3] a) during reentry on vehicle windward centerline, and b) heating rate used for preliminary analysis.

distributions. A one-dimensional finite element heat transfer analysis was done by Bapanapalli et al. [11]. The heat transfer analysis determined the maximum bottom face sheet temperature of the unit cell and the core temperature distribution at any particular reentry time. The core temperature distribution is plotted for three reentry times (450, 1575, and 1905 s) in Fig. 5a. The 1905-s reentry time corresponds to the time when maximum bottom face sheet temperature is reached.

Each temperature distribution resulted in thermal force resultants and thermal moments that caused the sandwich structure to linearly deform. In the case of laminated composites the thermal forces and moments were computed using Eq. (8)

$$[N^T, M^T] = \int_{-\frac{h}{2}}^{-\frac{h}{2}} [\bar{Q}]\{\alpha\}\Delta T[1, z]\mathrm{d}z \tag{8}$$

In Eq. (8), $[\bar{Q}]$ is the laminate stiffness matrix, $\{\alpha\}$ is the column matrix of the coefficient of thermal expansion and ΔT is the temperature change from the reference temperature. However, these equations do not apply to the present ITPS structure because there are no layers in the unit cell. Therefore, a micromechanics (homogenization) approach was used to determine the unit-cell thermal forces and moments. Consider the thermoelastic laminate constitutive relation

$$\begin{Bmatrix} N \\ M \end{Bmatrix} = [K]\begin{Bmatrix} \varepsilon_o \\ \kappa \end{Bmatrix} - \begin{Bmatrix} N^T \\ M^T \end{Bmatrix} \tag{9}$$

In Eq. (9), N^T and M^T are the unit cell's thermal force resultant and moment due to a temperature change of the ITPS. The thermal force resultants and moments are equal to the negative of forces and moments that act on the unit cell when it is completely constrained at its lateral boundary surfaces. An analytical procedure for predicting the ITPS thermal force and moment resultants are presented in this paper.

C. Thermal Force Resultants and Moments

An analytical method was developed to predict the thermal force and moment resultants acting on an ITPS sandwich panel from a given temperature distribution. Consider a unit cell made up of four composite laminates (two face sheets and two webs). Each laminate has its respective material properties and stiffness matrix. The unit cell was subjected to a temperature distribution $\Delta T(\bar{y})$ where $\bar{y}$ was the local axis of the inclined web starting from the top face. The temperature distribution equation was determined by fitting a quartic polynomial to the temperature distribution shown in Fig. 5a. A reference temperature at which the laminate is stress-free was assumed to be at room temperature and the temperatures in the faces were considered to be constant because the faces are thin when compared with the ITPS core thickness. Because of symmetry only half the unit cell was analyzed. The half-unit cell was constrained to prevent displacement in the x and y directions. The top face sheet had roller support in the z direction, which allowed the webs to expand in the $\bar{y}$ direction (Fig. 6a). The thermal problem was broken down into two problems. The first problem was the constrained problem in which force resultants that are equal and opposite to the component's (face or web) thermal forces were applied to the unit cell. This behavior is given by

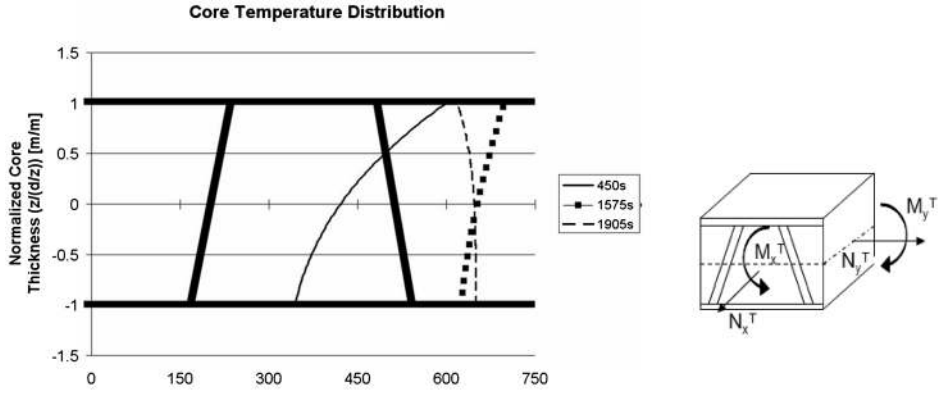

Fig. 5 a) Core temperature distribution at three reentry times, and b) resulting thermal force resultants and thermal moments.

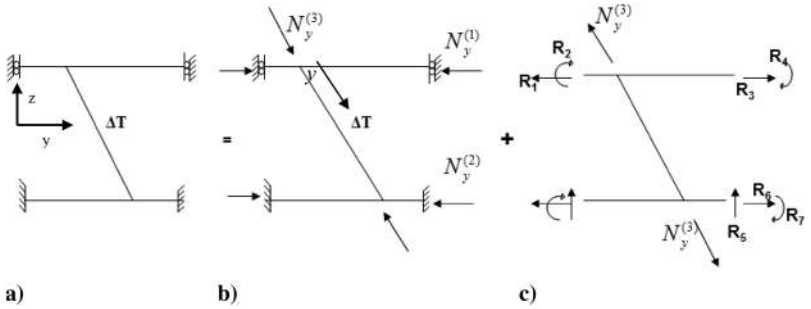

Fig. 6 a) Half-unit cell of the corrugated-core sandwich panel with a temperature distribution, b) constrained thermal problem, and c) unconstrained relaxed expansion.

$$[N_i]^{(e)} = [\bar{A}\ \bar{B}\ \bar{D}]\{0\} - \frac{1}{L}\int_{-\frac{s}{2}}^{\frac{s}{2}} \sum_{k=1}^{N} (Q_{ij}^{e})_k (z_k - z_{k-1})\Delta T(\bar{y})\mathrm{d}\bar{y} \quad (10)$$

The equal and opposite forces prevent any expansion in the half-unit cell; hence the strains are equal to zero. The average thermal force resultants were determined for the webs because the temperature distribution had a polynomial variation.

The second problem is an unconstrained half-unit cell with no temperature distribution, and the forces developed in the constrained problem, $N_y^{(1)}$, $N_y^{(2)}$, and $N_y^{(3)}$ are relaxed. The relaxed force resultants are equal and opposite to the force resultants obtained in Eq. (10). The constraints are represented by the reactions shown in Fig. 6c. The constraints are unknown reaction forces that were determined by Castigliano's second theorem [18]. The strain energy due to bending and normal force was considered. The strain energy of each component was determined and then summed to obtain the total strain energy in the half-unit cell. There are seven unknown reactions to be determined. To determine the seven unknown reactions seven boundary conditions were imposed, which are that the displacement and rotations due to each reaction are zero. The seven boundary conditions along with Castigliano's second theorem lead to a system of seven linear equations with seven unknowns

$$\frac{\partial U_s}{\partial R_i} = 0 \qquad i = 1, 2, 3 \ldots, 7 \quad (11)$$

Solving Eq. (11) leads to the solution of the seven reaction forces. By summing the x and y forces in Fig. 6c along with the x- and y-force resultant results from Fig. 6b, the desired thermal force resultant and moment for an ITPS sandwich panel were obtained. The relevant equations are given as follows:

$$N_y = R_3 + R_6 + (N_y^{(1)} + N_y^{(2)}) \quad (12)$$

$$M_y = R_4 + R_7 + \frac{d}{2}(N_y^{(1)} - N_y^{(2)}) + \frac{d}{2}(R_6 - R_3) \quad (13)$$

$$N_x = \frac{1}{2p}(N_x^{(1)}2p + N_x^{(2)}2p + N_x^{(3)}2s) \quad (14)$$

$$M_x = \left[\frac{d}{2}(N_x^{(1)} - N_x^{(2)})2p + \sum_{i=1}^{N} 2\left(z_i - \frac{d}{2}\right)N_x^{(3)}(i)\left(\frac{s}{N}\right)\right]\frac{1}{2p} \quad (15)$$

In Eq. (15), N is the number of discretization points in the web length. The force and moments resultants that are needed to constrain the unit cell during a change in temperature is equal to the negative of the thermal force resultants and moments of the ITPS as shown in Eq. (16)

$$[N^T, M^T] = [-N, -M] \quad (16)$$

D. Thermal Stress in the Faces and Webs

The analytical procedure was extended to obtain the thermal stresses in each component due to a given through-the-thickness temperature variation. According to classical laminate plate theory, the equations needed to determine thermal stresses are

$$\sigma = [\bar{Q}](\varepsilon - \alpha\Delta T) \quad (17)$$

To determine the thermal stresses in either the faces or the webs, the microthermal deformation of each component due to a unit-cell macrostrain or curvature must be known. The microdeformation of each component was determined by Eq. (3), which relates macro to microdeformation. The deformation transformation matrices that were derived by Martinez et al. [17] were used to determine microstrains and curvatures in the faces and webs (see for the transformation deformation matrices).

1. *Microthermal Stresses, Constrained Case*

The thermal stresses in the faces and webs were derived for an ITPS unit cell. The first case that was investigated was the constrained case where strains in the x and y directions were zero, however, the webs were free to expand in the web length direction and constrained in the x direction. The thermal stress equation for the constrained thermal expansion problem is shown in the following equation:

$$[\sigma] = -[\bar{Q}]\{\alpha\}\Delta T\left(\frac{-h}{2}, \frac{h}{2}\right) \quad (18)$$

Equation (18) is only valid for the top and bottom face sheets because the faces are fully constrained and the strains are zero. The webs, however, were not fully constrained and were allowed to expand in the $\bar{y}$ direction only. Therefore, an analytical solution for the web expansion under a fourth-order polynomial temperature distribution was derived. From Fig. 6a it can be seen that the constrained thermal problem for the half-unit cell was broken down into two individual problems. Problem 1 is Fig. 6b and problem 2 is Fig. 6c. The web strains in the $\bar{y}$ direction for problem one and problem two were determined and then summed to obtain the total web strain for the constrained thermal problem, which took into account the web expansion.

The web strain from problem-2 was obtained by determining the midplane strains and curvatures in the webs due to the reactions and relaxed forces (Fig. 7).

By summing the forces and moments in the $\bar{y}$ direction the equation that characterizes the force and moment at any location on the web was determined (refer to for the force and moment equation on the web). The midplane strain and curvature in the webs were determined by multiplying the force vector of the web with the inverse of the web's stiffness matrix, Eqs. (19) and (20)

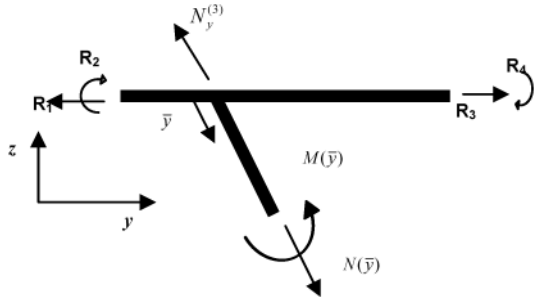

Fig. 7 Free body diagram of the top face sheet and web.

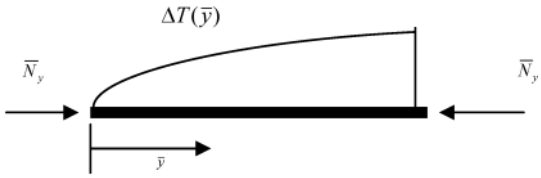

Fig. 8 Free body diagram of the webs with an average constraining force and a quartic temperature distribution.

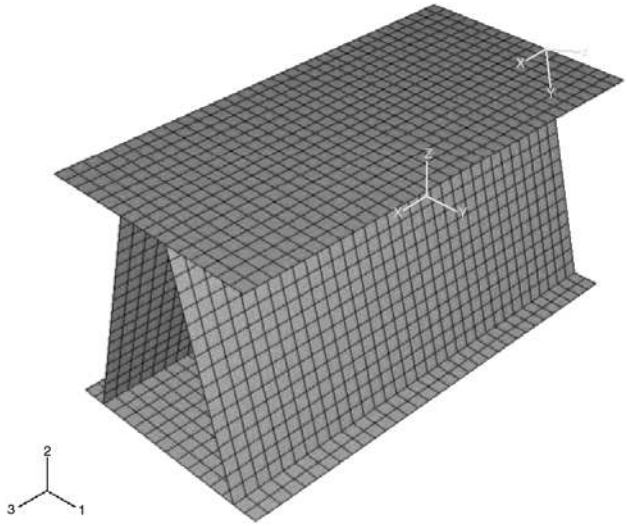

Fig. 9 Finite element model of the representative volume element.

$$\begin{Bmatrix} 0 \\ \varepsilon_{\bar{y}o} \\ 0 \\ 0 \\ \kappa_{\bar{y}} \\ 0 \end{Bmatrix} = \left(\begin{bmatrix} \bar{A} & \bar{B} \\ \bar{B} & \bar{D} \end{bmatrix}^{-1} \right)^{(\text{Web})} \begin{Bmatrix} N_x \\ N_y \\ N_{xy} \\ M_x \\ M_y \\ M_{xy} \end{Bmatrix} \tag{19}$$

$$\varepsilon_{\bar{y}o}(\bar{y}) = \left(\frac{-A_{12}^{*^2}}{A_{11}^*} + A_{22}^* \right) N(\bar{y}) \qquad \kappa_{\bar{y}}(\bar{y}) = \left(\frac{-D_{12}^{*^2}}{D_{11}^*} + D_{22}^* \right) M(\bar{y}) \tag{20}$$

The web strain for problem-1 was determined by first modeling the free body diagram of the web only from Fig. 6b. The webs are constrained by a compressive force from Eq. (10), which was the average force needed to constrain the web in the web length direction. However, the average displacement was zero, but the local displacements and local strains were not zero because of the fourth-order polynomial of the temperature distribution, which causes local thermal strains. An analytical equation was derived that accounts for the expansion of the web due to a temperature distribution through the web length.

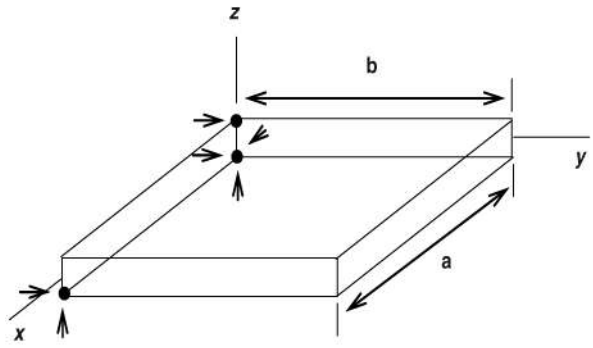

a)

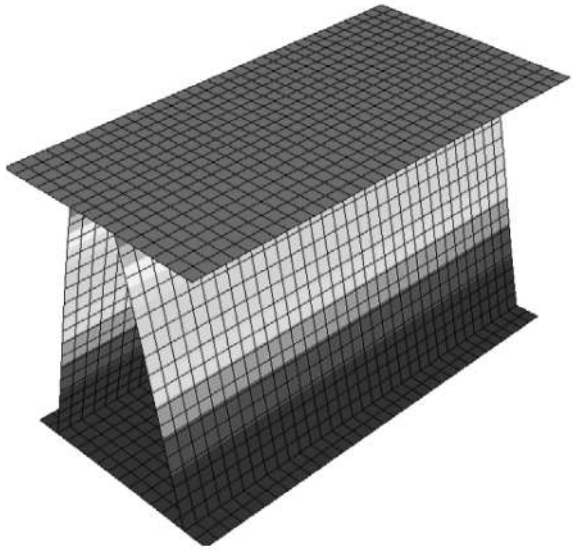

b)

Fig. 10 a) Boundary conditions imposed on the plate to prevent rigid body motion. An arrow pointing at a black dot indicates that the displacement of that point is fixed in the direction of the arrow. b) Deformation of the unit cell due to temperature distribution with the unit cell fully constrained.

Considering only the $\bar{y}$ direction, which accounts for web length expansion from Fig. 8, and using the constitutive relation results in the following equation:

$$\bar{N}_{\bar{y}} = \bar{A}_{22}\varepsilon_{yo} - \hat{N}\Delta T(\bar{y}) \tag{21}$$

where

$$\hat{N} = \int_{-\frac{h}{2}}^{\frac{h}{2}} \bar{Q}\alpha \, \mathrm{d}z \tag{22}$$

Table 1 Periodic displacement boundary conditions imposed on the lateral faces of unit cell for in-plane strains and curvatures

$u(a,y)-$ $u(0,y)$	$v(a,y)-$ $v(0,y)$	$w(a,y)-$ $w(0,y)$	$u(x,b)-$ $u(x,0)$	$v(x,b)-$ $v(x,0)$	$w(x,b)-$ $w(x,0)$	$\theta_x(a,y)-$ $\theta_x(0,y)$	$\theta_y(a,y)-$ $\theta_y(0,y)$	$\theta_x(x,b)-$ $\theta_x(x,0)$	$\theta_y(x,b)-$ $\theta_y(x,0)$
$a\varepsilon_{x0}+$ $az\kappa_x$	$a/2\gamma_{xy0}+$ $az/2\kappa_{xy}$	$-a^2/2\kappa_x-$ $ay/2\kappa_{xy}$	$b/2\gamma_{xy0}+$ $bz/2\kappa_{xy}$	$b\varepsilon_{y0}+bz\kappa_y$	$-b^2/2\kappa_y-$ $bx/2\kappa_{xy}$	$-a/2\kappa_{xy}$	$a\kappa_x$	$-b\kappa_y$	$b/2\kappa_{xy}$

Table 2 Non-zero thermal forces in the unit cell due to thorough thickness temperature distribution

	N_x, N/m	N_y, N/m	M_x, N m/m	M_y, N m/m
Analytical	581.03	317.48	10.97	11.41
Finite element	563.88	316.77	11.48	11.45
% diff.	3.04%	0.22%	4.36%	0.38%

The differential equation of equilibrium for Fig. 8 is

$$\frac{\partial \bar{N}_{xy}}{\partial \bar{x}} + \frac{\partial \bar{N}_y}{\partial \bar{y}} = 0 \tag{23}$$

Substituting Eq. (21) into Eq. (23) results

$$\bar{A}_{22}\frac{\partial^2 \bar{v}}{\partial \bar{y}^2} - \hat{N}\frac{\partial}{\partial \bar{y}}\Delta T(\bar{y}) = 0 \tag{24}$$

Integrating Eq. (24) twice with respect to $\bar{y}$, the web displacement as a function of $\bar{y}$ was obtained

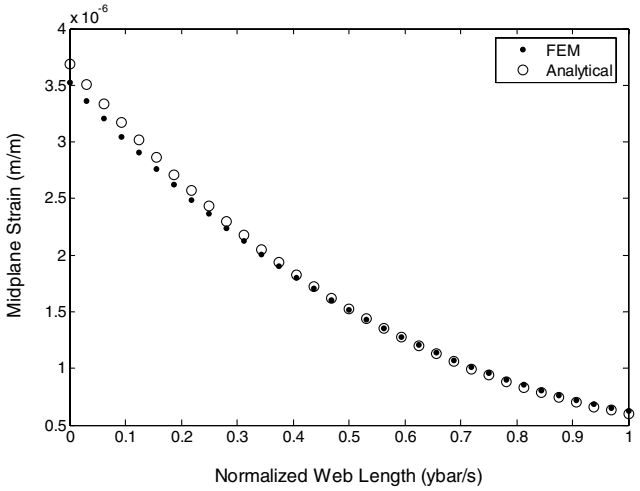

Fig. 11 Web strain expansion for the constrained thermal problem.

$$\bar{v}(\bar{y}) = \iint \frac{\hat{N}}{\bar{A}_{22}}\frac{\partial}{\partial \bar{y}}\Delta T(\bar{y})\,d\bar{y}\,d\bar{y} + D\bar{y} + E \tag{25}$$

Equation (25) has two unknown constants that were solved by considering two boundary conditions.

$$\bar{v}(0) = 0 \qquad \bar{v}(s) = 0 \tag{26}$$

Substituting Eq. (25) into Eq. (26) and solving for the system of linear equations, the unknown constants D and E were determined. Finally, taking the partial derivative of Eq. (25) with respect to $\bar{y}$, the web midplane strain in the $\bar{y}$ direction for problem-1 was obtained

$$\varepsilon_{yo}(\bar{y}) = \frac{\partial \bar{v}}{\partial \bar{y}} = \frac{\partial}{\partial \bar{y}}\left[\iint \frac{\hat{N}}{\bar{A}_{22}}\frac{\partial}{\partial \bar{y}}\Delta T(\bar{y})\,d\bar{y}\,d\bar{y} + D\bar{y} + E\right] \tag{27}$$

Summing the strain obtained from Eqs. (20) and (27) yields the web strain in the web length direction for the constrained problem with consideration of web expansion.

2. Thermal Stresses, Unconstrained Case

In this section the stresses in the faces and webs due to the force resultants obtained from Eqs. (12–15) were determined. Using the thermal force vector from Eq. (16) and multiplying the result with the unit-cell stiffness, Eq. (7) yields the thermal strain and curvature for the unit cell

$$\begin{Bmatrix} \varepsilon_o \\ \kappa \end{Bmatrix}^M = [K]^{-1}\begin{Bmatrix} -N \\ -M \end{Bmatrix} \tag{28}$$

Equation (28) solves the unit-cell strain and curvature under thermal loading. Using the result in Eq. (28) along with the deformation transformation matrix for the faces and the refined web stress deformation transformation matrix [17], the microdeformation of the faces and webs was determined, Eq. (3). The microdeformations are the local strains and curvature that the faces or the webs will undergo due to the temperature distribution. The face and web stresses were determined by multiplying the microdeformation from Eq. (28) with its respective transformed lamina stiffness matrix

$$[\sigma]^{(e)} = [\bar{Q}]^{(e)}[T_D]^{(e)}[K]^{-1}\begin{bmatrix} N^T \\ M^T \end{bmatrix} \tag{29}$$

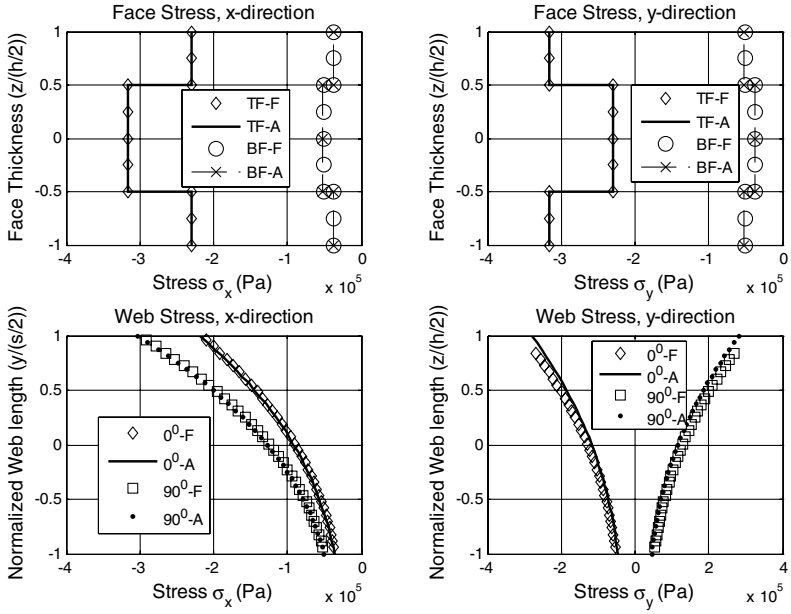

Fig. 12 Stresses in the *x* and *y* directions in the top face, bottom face, and web for the constrained thermal problem. *A* represents analytical results and *F* represents finite element results. The 0 and 90 indicate the ply orientation.

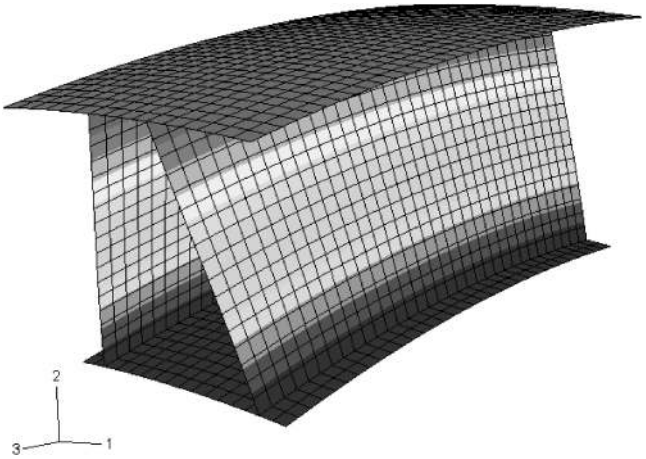

Fig. 13 Deformation of the unit cell due to the unconstrained boundary condition.

IV. Results

A. Thermal Force Resultant and Moment

For verification of the effectiveness of the analytical models, consider a corrugated-core sandwich panel unit cell with the following dimensions: $p = 50$ mm, $d = 100$ mm, $t_{\mathrm{TF}} = 1$ mm, $t_{\mathrm{BF}} = 1$ mm, $t_w = 1$ mm, and $\theta = 75°$. In the example the properties of the graphite/epoxy composite are assumed to be that of AS/Epoxy ($E_1 = 138$ GPa, $E_2 = 9$ GPa, $\nu_{12} = 0.3$, $G_{12} = 6.9$ GPa), The web and the face sheets are assumed to contain four laminas with the stacking sequence $[(0/90)_2]$. The representative volume element or unit cell used in the homogenization is shown in Fig. 9. A finite element analysis was conducted on the unit cell using the commercial ABAQUS$^{\mathrm{TM}}$ finite element program. Eight node shell elements were used to model the face sheets and the webs. The shell elements have the capability to include multiple layers of different material properties and thickness. Three integration points were used through the thickness of the shell elements. The FEM model consisted of 6666 nodes and 2178 elements.

Known strains and curvatures were imposed on the unit cell. The force and moment resultants were calculated from the resulting stresses after the analysis. Strains were imposed by enforcing periodic displacement boundary conditions on the unit cell as shown in Table 1. To prevent rigid body motion and translation, the unit cell (Fig. 10) was subjected to minimum support constraints. The top and bottom surfaces were assumed to be free of traction. The faces $x = 0$ and $x = a$ have identical nodes on each side as well as the other faces $y = 0$ and $y = b$. The identical nodes on the opposite faces are constrained to enforce the periodic boundary conditions. Figure 10 shows the deformations of the unit cell as a result of imposing the periodic boundary conditions. The strains and curvature in Table 1 are set to zero to prevent expansion of the unit cell in the x and y direction. The 450 s temperature distribution (Fig. 5a) was imposed on the FE model. The resulting force and moment resultant needed to constrain the unit cell when subjected to a temperature distribution will be equal to the negative of the thermal forces.

The nodal forces of the boundary nodes were determined from the stress finite element output after the analyses. Then the force and moment resultants acting on the unit cell were obtained from the nodal forces using Eq. (30). The resultants obtained are the forces needed to constrain the unit cell, and they will be equal to the negative of the thermal forces. The results are shown in Table 2

$$[N_i, M_i] = \left(\frac{1}{b}\right) \sum_{m=1}^{n} [1, z] F_i^{(m)}(a, y, z) \tag{30}$$

The finite element results in Table 2 indicate that the maximum difference between exact thermal forces and those predicted by Eqs. (12–15) is less than 5% difference.

B. Thermal Stress Verification

1. Constrained Case

Consider the same FEM unit cell representative volume element and mesh from Fig. 9 with the same material properties and cross ply layup. All strains in the x direction are zero and all strains in the $y$direction are zero for the unit cell (Table 1). The unit cell was subjected to the 450 s temperature distribution that was illustrated in Fig. 5a. The web was allowed to expand by the addition of rollers as shown in Fig. 6a. The strains in the webs were extracted from the finite element output after analysis. Figure 11 compares the finite element and analytical results for web strains.

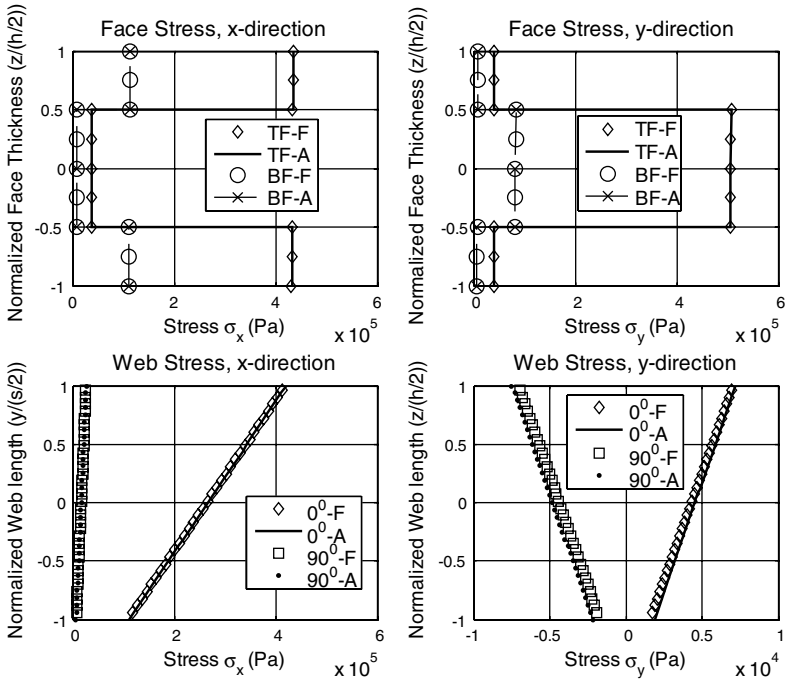

Fig. 14 Stresses in the x and y directions in the top face (TF), bottom face (BF) and web for the unconstrained thermal problem. *A* represents analytical results and *F* represents finite element results. The 0 and 90 represent the ply orientation.

The results in Fig. 11 indicate that the analytical procedure developed to obtain the strain in the $\bar{y}$ direction, which accounts for the free expansion of the webs [Eqs. (20) and (27)] yields a less than 2% difference strain result when compared with the FE results, which yield less than 5% stress results when compared with finite element results, Fig. 12. Correct strain results are necessary to obtain accurate stress results.

2. Unconstrained Case

The same FEM model of the representative volume element shown in Fig. 9 with the same material properties and cross-ply layup was investigated for this case. For this example, periodic thermal strains from Eq. (28) were applied to the finite element model. The stress results from the analytical and finite element analysis were compared in the x and y directions. The results from Eq. (28) were substituted in Table 1 and inputted into the FE model to obtain the appropriate periodic displacement boundary conditions for the unconstrained thermal problem. Figure 13 illustrates the deformation of the unit cell after appropriately applying the periodic thermal boundary conditions. The maximum difference in stresses from the analytical and the finite element methods is within 5%. The results indicate that the thermal force resultants from Eqs. (12–15) was an efficient and fast way to determine thermal forces and moments as well as stresses in the faces or webs (Fig. 14) from an applied unit-cell force resultant or moment.

V. Conclusions

The truss-core sandwich panel, which is a candidate structure for ITPS, is homogenized as an equivalent orthotropic plate. Detailed formulation of the bending, extensional, coupling, and shear stiffness for an ITPS unit cell was presented. The ITPS will experience extreme reentry temperatures that will result in thermal moments and force resultants on the ITPS unit cell. A micromechanics approach was developed to determine unit-cell thermal forces and moments. The analytical model can be used to determine thermal forces and moments for the ITPS unit cell, which can lead to accurate thermal strains and stress. The results between finite element analysis and the analytical model for the constrained and unconstrained thermal problem were within 5% of each other, thus validating the method.

Appendix

The transformation matrix for the top face sheet is

$$\{D\}^{(1)} = T_D^1\{D\}^M$$

$$\begin{Bmatrix} \varepsilon_{xo} \\ \varepsilon_{yo} \\ \gamma_{xyo} \\ \kappa_x \\ \kappa_y \\ \kappa_{xy} \end{Bmatrix}^{(1)} = \begin{bmatrix} 1 & 0 & 0 & \frac{d}{2} & 0 & 0 \\ 0 & 1 & 0 & 0 & \frac{d}{2} & 0 \\ 0 & 0 & 1 & 0 & 0 & \frac{d}{2} \\ 0 & 0 & 0 & 1 & 0 & 0 \\ 0 & 0 & 0 & 0 & 1 & 0 \\ 0 & 0 & 0 & 0 & 0 & 1 \end{bmatrix} \begin{Bmatrix} \varepsilon_{xo} \\ \varepsilon_{yo} \\ \gamma_{xyo} \\ \kappa_x \\ \kappa_y \\ \kappa_{xy} \end{Bmatrix}^{(M)} \tag{A1}$$

The transformation matrix for the bottom face sheet is

$$\{D\}^{(2)} = T_D^2\{D\}^M$$

$$\begin{Bmatrix} \varepsilon_{xo} \\ \varepsilon_{yo} \\ \gamma_{xyo} \\ \kappa_x \\ \kappa_y \\ \kappa_{xy} \end{Bmatrix}^{(1)} = \begin{bmatrix} 1 & 0 & 0 & -\frac{d}{2} & 0 & 0 \\ 0 & 1 & 0 & 0 & -\frac{d}{2} & 0 \\ 0 & 0 & 1 & 0 & 0 & -\frac{d}{2} \\ 0 & 0 & 0 & 1 & 0 & 0 \\ 0 & 0 & 0 & 0 & 1 & 0 \\ 0 & 0 & 0 & 0 & 0 & 1 \end{bmatrix} \begin{Bmatrix} \varepsilon_{xo} \\ \varepsilon_{yo} \\ \gamma_{xyo} \\ \kappa_x \\ \kappa_y \\ \kappa_{xy} \end{Bmatrix}^{(M)} \tag{A2}$$

The transformation matrix for the left web is

$$\{D\}^{(e)} = T_D^e\{D\}^M \qquad \begin{Bmatrix} \varepsilon_{\bar{x}o} \\ \varepsilon_{\bar{y}o} \\ \gamma_{\bar{x}\bar{y}o} \\ \kappa_{\bar{x}} \\ \kappa_{\bar{y}} \\ \kappa_{\bar{x}\bar{y}} \end{Bmatrix}^{(3)} = \begin{bmatrix} 1 & 0 & 0 & (\frac{d_c}{2} - \bar{y}\sin\theta) & 0 & 0 \\ \nu & 0 & 0 & \upsilon(\frac{d_c}{2} - \bar{y}\sin\theta) & 0 & 0 \\ 0 & 0 & -f(p, d, t_{\mathrm{TF}}, t_{\mathrm{BF}}, t_w, \theta) & 0 & 0 & 0 \\ 0 & 0 & 0 & -\cos\theta & 0 & 0 \\ 0 & 0 & 0 & 0 & -g(p, d, t_{\mathrm{TF}}, t_{\mathrm{BF}}, t_w, \theta) & 0 \\ 0 & 0 & 0 & 0 & 0 & 1 \end{bmatrix} \begin{Bmatrix} \varepsilon_{xo} \\ \varepsilon_{yo} \\ \gamma_{xyo} \\ \kappa_x \\ \kappa_y \\ \kappa_{xy} \end{Bmatrix}^{(M)} \tag{A3}$$

The transformation matrix for the right web is

$$\{D\}^{(e)} = T_D^e\{D\}^M \qquad \begin{Bmatrix} \varepsilon_{\bar{x}o} \\ \varepsilon_{\bar{y}o} \\ \gamma_{\bar{x}\bar{y}o} \\ \kappa_{\bar{x}} \\ \kappa_{\bar{y}} \\ \kappa_{\bar{x}\bar{y}} \end{Bmatrix}^{(3)} = \begin{bmatrix} 1 & 0 & 0 & (\frac{d_c}{2} - \bar{y}\sin\theta) & 0 & 0 \\ \nu & 0 & 0 & \upsilon(\frac{d_c}{2} - \bar{y}\sin\theta) & 0 & 0 \\ 0 & 0 & f(p, d, t_{\mathrm{TF}}, t_{\mathrm{BF}}, t_w, \theta) & 0 & 0 & 0 \\ 0 & 0 & 0 & -\cos\theta & 0 & 0 \\ 0 & 0 & 0 & 0 & g(p, d, t_{\mathrm{TF}}, t_{\mathrm{BF}}, t_w, \theta) & 0 \\ 0 & 0 & 0 & 0 & 0 & 1 \end{bmatrix} \begin{Bmatrix} \varepsilon_{xo} \\ \varepsilon_{yo} \\ \gamma_{xyo} \\ \kappa_x \\ \kappa_y \\ \kappa_{xy} \end{Bmatrix}^{(M)} \tag{A4}$$

The normal force and moment web equations as a function of $\bar{y}$ obtained from Fig. 10 are

$$N(\bar{y}) = N_y^{(3)} - R_1\cos\theta - R_3\cos\theta \tag{A5}$$

$$M(\bar{y}) = (R_3 + R_1)\bar{y}\sin\theta + R_2 + R_4 \tag{A6}$$

Acknowledgment

This research is sponsored by the Constellations University Institutes Project. The program manager is Claudia Mayer at NASA Glenn Research Center.

References

[1] Blosser, M. L., "Advanced Metallic Thermal Protection Systems for Reusable Launch Vehicles," Ph.D. Dissertation, Mechanical and Aerospace Dept., Univ. of Virginia, Charlottesville, VA, 2000.

[2] Behrens, B., and Muller, M., "Technologies for Thermal Protection Systems applied on re-usable launcher," *Acta Astronautica*, Vol. 55, Nos. 3–9, Aug.–Nov. 2004, pp. 529–536. doi:10.1016/j.actaastro.2004.05.034

[3] Dorsey, J. T., Poteet, C. C., Wurster, K. E., and Chen, R. R., "Metallic Thermal Protection System Requirements, Environments, and Integrated Concepts," *Journal of Spacecraft and Rockets*, Vol. 41, No. 2, March–April 2004, pp. 162–172. doi:10.2514/1.9173

[4] Blosser, M. L., "Development of Metallic Thermal Protection Systems for the Reusable Launch Vehicle," NASA TM-110296, Oct. 1996.

[5] Lok, T. S., and Cheng, Q., "Elastic Stiffness Properties and Behavior of Truss-Core Sandwich Panel," *Journal of Structural Engineering*, Vol. 126, No. 5, May 2000, pp 552–559. doi:10.1061/(ASCE)0733-9445(2000)126:5(552)

[6] Valdevit, L., Hutchinson, J. W., and Evans, A. G., "Structurally Optimized Sandwich Panels with Prismatic Cores," *International Journal of Solids and Structures*, Vol. 41, May 2004, pp. 5105–5124. doi:10.1016/j.ijsolstr.2004.04.027

[7] Nordstrand, T., "On Buckling Loads for Edge-Loaded Orthotropic Plates Including Transverse Shear," *Composite Structures*, Vol. 65, No. 1, 2004, pp. 1–6.

[8] Biancolini, M. E., "Evaluation of Equivalent Stiffness Properties of Corrugated Board," *Composite Structures*, Vol. 69, No. 3, 2005, pp. 322–328. doi:10.1016/j.compstruct.2004.07.014

[9] Buannic, N., Cartraud, P., and Quesnel, T., "Homogenization of Corrugated Core Sandwich Panels," *Composite Structures*, Vol. 59, No. 3, 2003, pp. 299–312. doi:10.1016/S0263-8223(02)00246-5

[10] Tan, K. H., Fung, T. C., and Lok, T. S., "A Simplified Thick Plate Analysis of All-Steel Sandwich Panels," *Journal of Structural Engineering*, Vol. 71, No. 14, 1993, pp. 253–258.

[11] Bapanapalli, S. K., Martinez, O., Sankar, B. V., Haftka, R. T., and Blosser, M. L., "Analysis and Design of Corrugated-Core Sandwich Panels for Thermal Protection Systems of Space Vehicles," *47th AIAA/ASME/ASCE/AHS/ASC Structures, Structural Dynamics, and Materials Conference*, AIAA, Reston, VA, May 2006.

[12] Libove, C. and Hubka, R. E., "Elastic Constants for Corrugated Core Sandwich Plates," National Advisory Committee for Aeronautics, Technical Note (NACA TN)-2289, 1951.

[13] Fung, T. C., Tan, K. H., and Lok, T. S., "Analysis of *C*-Core Sandwich Plate Decking," *Proceedings of the 3rd International Offshore and Polar Engineering Conference*, International Society of Offshore and Polar Engineers, Republic of Singapore, Vol. 4, 1993, pp. 244–249.

[14] Fung, T. C., Tan, K. H., and Lok, T. S., "Elastic Constants for *Z*-core sandwich panels," *Journal of Structural Engineering, ASCE*, Vol. 120, No. 10, 1994, pp 3046–3065. doi:10.1061/(ASCE)0733-9445(1994)120:10(3046)

[15] Vinson, J. R., *The Behavior of Sandwich Structures of Isotropic and Composite Materials*, Technomic, Lancaster, PA, 1999.

[16] Whitney, M., *Structural Analysis of Laminated Anisotropic Plates*, Technomic, Lancaster, PA, 1987.

[17] Martinez, O., Sankar, B. V., Haftka, R., Blosser, M., and Bapanapalli, S. K., "Micromechanical Analysis of a Composite Corrugated-Core Sandwich Panel for Integral Thermal Protection Systems," *AIAA Journal*, Vol. 45, No. 9, pp. 2323–2336. doi:10.2514/1.26779

[18] Hibbeler, R. C., *Mechanics of Materials*, 4th ed., Prentice Hall, Upper Saddle River, NJ, 1999, p. 705.

R. Kapania
Associate Editor